InP-on-Si Optically Pumped Microdisk Lasers via Monolithic Growth and Wafer Bonding

Svenja Mauthe, *Student Member, IEEE*, Noelia Vico Triviño, Yannick Baumgartner, *Student Member, IEEE*, Marilyne Sousa, Daniele Caimi, Thilo Stöferle, Heinz Schmid, *Member, IEEE*, and Kirsten Emilie Moselund, *Senior Member, IEEE*

***Abstract*—On-chip optical light sources are key components in photonic integrated circuits and optical communication. In this paper, we use a novel integration technique called template-assisted selective epitaxy (TASE) to monolithically integrate InP microdisk lasers on silicon. TASE offers several advantages for new device concepts such as lateral doping, dense co-integration of different III–V materials, and in-plane integration with silicon electronics and passive components. Here, we demonstrate room-temperature lasing from InP hexagonal microdisks integrated via TASE. In order to assess and evaluate the viability of TASE, a second InP hexagonal microdisk sample is prepared for comparison using the highly developed and mature direct wafer bonding technique. The lasing performance of the TASE monolithic devices and the bonded microdisk devices is investigated under pulsed optical pumping as a function of temperature and compared. The lasing threshold as well as the light-in light-out curves of our TASE structures compare favorably with the bonded InP hexagonal microdisks. This demonstrates that our TASE approach is a promising technique for the monolithic integration of optical devices on Si.**

***Index Terms*—Heterogeneous integration, III–V materials on silicon, microdisk lasers, optical pumping, semiconductor lasers.**

I. Introduction

EFFICIENT integrated micro- and nano-sized light sources have attracted great attention due to their application in dense photonic integrated circuits (PICs), sensing, and optical communication [1], [2]. PICs can boost the performance of existing complementary metal-oxide-semiconductor electronic circuit (CMOS) technology and allow for more complex electro-optical functionalities for both on-chip and off-chip applications. In order to achieve a dense integration of highly efficient light sources on Si, which has an indirect bandgap, new materials and designs are required. III-V microdisk lasers represent excellent candidates due to their small integration foot print, high-quality factors, and their relatively easy cavity fabrication. Major progress has been made in the direct integration of defect-free III-V gain material on Si and hence, overcoming the significant lattice and thermal mismatch [3], [4]. Small foot print lasers have been demonstrated using integration techniques such as wafer bonding [5], [6], buffered layer growth [7]–[9], nanowire growth [10], [11], and shallow-trench-isolation (STI) growth [12]–[15]. So far, direct wafer bonding of either discrete components or a full III-V stack represents the most advanced approach to integrate III-Vs on silicon for photonic applications. However, although direct wafer bonding has advanced quickly in the last years, the process is not yet truly compatible on wafer scale due to a mismatch in wafer size. Moreover, for many applications a seamless integration of III-Vs with silicon photonics at the individual device level is required and hence, direct monolithic growth would be beneficial. We recently developed an epitaxial integration method called template-assisted selective epitaxy (TASE [16], [17]) which allows for the seamless monolithic integration of high quality III-V material at lithographically defined positions for electrical and optical applications [18]. Using this technique, we recently demonstrated room-temperature lasing of hexagonal GaAs microdisks and low-temperature lasing of circular InGaAs microdisks [19], [20].

In this work, we extend our approach to InP which allows for future integration of lattice-matched quantum wells (QWs) and hence, an emission wavelength beyond the Si absorption gap as conceptionally shown in [21]. However, the monolithic integration of InP on Si is more challenging than for GaAs due to a larger lattice mismatch of 8% and a difference of 84% in thermal expansion coefficient [22]. Here we demonstrate single crystalline InP microdisk lasers integrated on Si (111) via TASE and thoroughly characterized using photoluminescence (PL) spectroscopy, scanning electron microscopy (SEM), and scanning transmission electron microscopy (STEM). The Si (111) substrate enables the formation of hexagonal shaped InP microdisks with smooth $\{110\}$ sidewalls. However, as demonstrated with GaAs, growth from a (001) substrate is also possible [19]. In order to assess and compare quantitatively the performance of the TASE-integrated microdisks, similar sized and shaped InP structures are fabricated via direct wafer bonding. All devices are fabricated and characterized in house which allows for a thorough direct comparison between the fabrication approaches and an evaluation of the performance of TASE for future photonic integration.

Manuscript received February 1, 2019; revised April 12, 2019; accepted April 30, 2019. Date of publication May 10, 2019; date of current version June 10, 2019. This work was supported in part by Horizon 2020 Project PLASMIC under Grant 678567 and in part by Horizon 2020 Project DIMENSION under Grant 688003. *(Corresponding author: Svenja Mauthe.)*

The authors are with IBM Research—Zurich, 8803 Rueschlikon, Switzerland (e-mail: svm@zurich.ibm.com; nvi@zurich.ibm.com; umg@zurich.ibm.com; sou@zurich.ibm.com; cai@zurich.ibm.com; tof@zurich.ibm.com; sih@zurich.ibm.com; kmo@zurich.ibm.com).

Color versions of one or more of the figures in this paper are available online at http://ieeexplore.ieee.org.

Digital Object Identifier 10.1109/JSTQE.2019.2915924

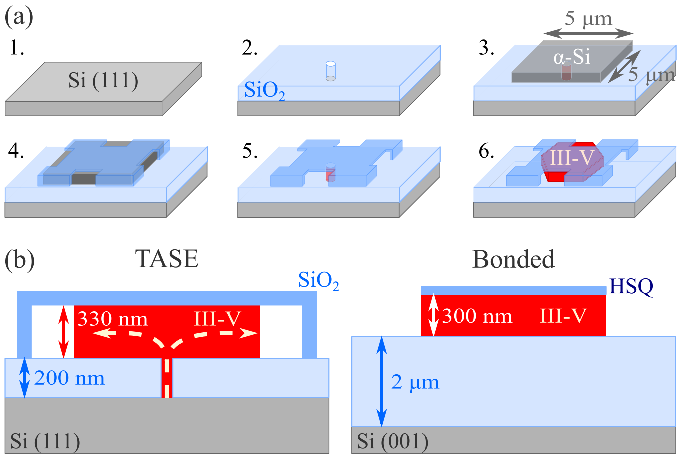

Fig. 1. (a) TASE fabrication steps: (1) Si (111) substrate. (2) Deposition and patterning of a silicon oxide layer. (3) Deposition and patterning of α-Si layer. (4) Deposition and patterning of template oxide. (5) Etching of the α-Si layer. (6) Growth of the III-V material by MOCVD. (b) Schematic cross-section of a TASE (left) and bonded (right) microdisk. The dashed arrows indicate the growth direction during TASE growth. Schematics are not drawn to scale.

II. Integration of InP Microdisk Lasers on Si

Samples are fabricated using two different integration techniques, namely TASE and direct wafer bonding. The active material for both fabrication approaches has been grown in our metal-organic chemical vapor deposition (MOCVD) reactor at 550 °C and a V/III ratio of ~70.

A. Template-Assisted Selective Epitaxy

The monolithic integration based on TASE is done as follows. First, a 200 nm thick oxide layer is deposited on a Si (111) substrate by plasma-enhanced chemical vapor deposition (PECVD). This thickness provides a compromise between sufficient optical isolation of the optical mode in the III-V material from the Si substrate while enabling a high InP nucleation yield. Next, small openings of 200 nm × 200 nm are patterned and etched down to the Si (111) substrate (see step 2 in Fig. 1(a)). In order to assure a clean and smooth Si surface for the InP nucleation, a short diluted tetramethylammonium hydroxide (TMAH) etch is performed. First, we grow InP nucleation seeds inside the pre-defined openings onto the Si substrate using MOCVD growth (~100 nm, not depicted in the schematics). By performing this separate InP nucleation growth, a high nucleation yield is achieved. Subsequently, a 3 nm Al_2O_3 protection layer and a sacrificial amorphous Si (α-Si) layer of 300 nm are deposited. The α-Si is patterned and covered with 200 nm oxide, shaping the cavity for the subsequent III-V growth (steps 3 and 4 in Fig. 1(a)). After partially opening the oxide layer the underlying α-Si is etched and a hollow cavity forms, exposing the small InP nucleation seed (Fig. 1(a) step 5). The Al_2O_3 protection layer is etched in a short DHF (diluted hydrofluoric acid) dip. In a final step, InP is grown inside the hollow cavity from the small InP nucleation seed using MOCVD (step 6 in Fig. 1(a)). By varying the growth duration, the diameter of the disks can be controlled.

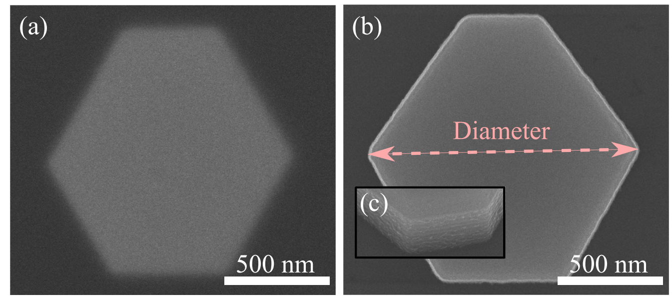

Fig. 2. SEM images of (a) TASE and (b) bonded and etched InP microdisk. The TASE image is blurry since it is taken with the 200 nm oxide template on top. The dashed line in (b) marks the diameter of the structure as referred to in this paper. The inset (c) shows the sidewalls of the 300 nm thick bonded structure in (b) after etching.

B. Direct Wafer Bonding

A second sample is prepared using a direct wafer bonding approach. This allows for a thorough comparison and evaluation of our approach since bonding is one of the most advanced integration techniques for III-Vs on Si. In this direct wafer bonding approach, the active InP material (300 nm) is grown onto a sacrificial InP wafer with a lattice-matched InGaAs etch stop and subsequently bonded to a Si (001) wafer with 2 μm oxide layer. Due to the lattice-matched growth of the active InP layer a defect-free gain layer of high crystal quality can be achieved. Details on the bonding process can be found in [23]. Next, the sacrificial InP substrate and the etch stop layer are removed. The final InP layer is patterned and etched using hydrogen silsesquioxane (HSQ) and an inductively coupled plasma (ICP) dry etch. A short wet etch is performed to clean the surface after the dry etching. Further surface passivation or surface termination is not performed. The masking HSQ layer is not removed in order to act as a top oxide layer similar to the template oxide for the TASE structures.

In order to permit quantitative comparison between the microdisks, structures etched in the bonded InP layer resemble the shape and size of the TASE structures. SEM images of the TASE-grown and bonded InP structures show the geometry of the individual microdisks (see Fig. 2(a) and (b)). Both samples exhibit a hexagonal shape with similar diameters of ~1.22 μm and ~1.28 μm for the TASE and bonded structures, respectively. We define the diameter of our hexagons as the distance marked in Fig. 2(b). Moreover, both samples are covered with an oxide layer on top of the InP structure. An important figure is the thickness of the InP layer. By design, both InP layers are 300 nm thick. Due to a short DHF dip before the III-V growth during TASE, the empty oxide cavity is slightly expanded resulting in a final InP thickness of 330 nm. A schematic overview of the cross section of both structures indicating their similarities and differences can be found in Fig. 1(b).

III. Material Characterization

SEM images of the TASE-grown and bonded InP structures are depicted in Fig. 2(a) and (b), respectively. The SEM image in Fig. 2(a) shows a hexagonal shape of the TASE structure which

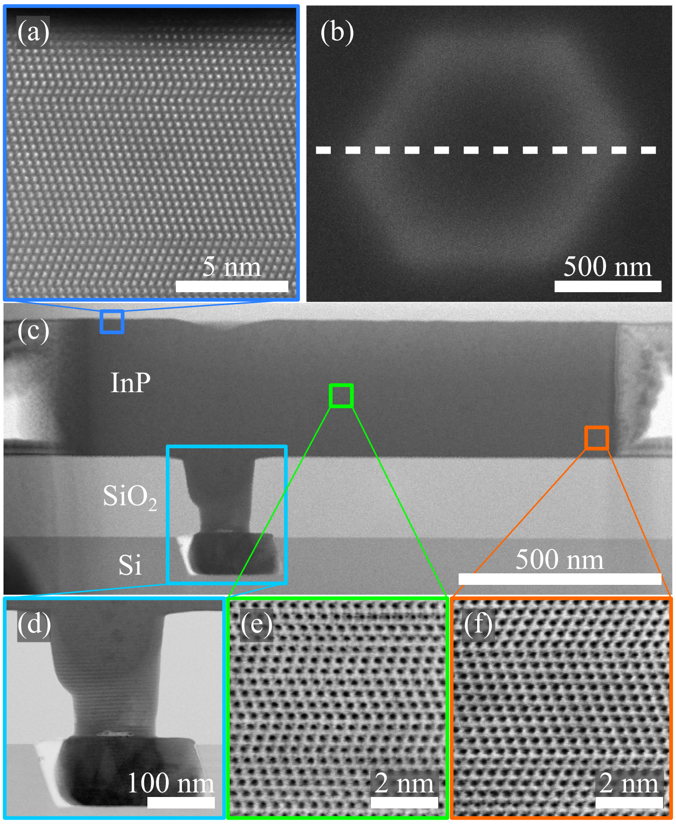

Fig. 3. Top view SEM (b) and cross-section STEM (c) image of a TASE-grown microdisk. (d) Close-up view of the Si/InP nucleation interface and the stem. High resolution bright field images taken at the marked positions in (c) are depicted in (a), (e), and (f).

speaks for an epitaxial relationship with the Si (111) substrate. In order to confirm the single crystallinity of the TASE structure, STEM is performed. Using Ga focused-ion beam etching (FIB), we prepare a thin lamella of the TASE structure along the dashed line depicted in Fig. 3(b). Next, STEM characterization is performed using a double spherical aberration corrected JEOL ARM200F microscope operated at 200 kV. Fig. 3(c) shows a cross-section overview featuring vertical {110} sidewalls and a hexagonal top (111) surface which indicates the alignment to the (111) Si substrate. The structure is located on top of 200 nm SiO_2 and connected to the Si substrate through a stem in the oxide layer. During the growth, InP nucleates at the Si interface, grows into the oxide stem, and expands into the empty oxide template as sketched in Fig. 1. The short TMAH dip performed before the InP growth etches the Si substrate and results in an undercut region underneath the oxide trench. At the Si/III-V interface, extended defects, like twin planes, stacking faults, and point defects, are observed. However, due to the confinement of the growth when reaching the stem in the oxide layer, these defects are terminated and do not propagate further (see Fig. 3(d)). High-resolution STEM images are taken at multiple locations throughout the crystal as illustrated in Fig. 3(a), (e), and (f). All images show the same crystal orientation of the InP and hence, confirm a single crystalline structure. Additionally, they reveal twin axes, as well as, short wurtzite segments.

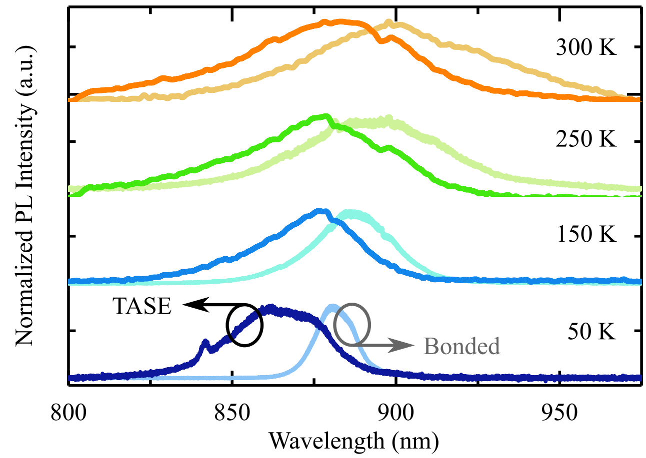

Fig. 4. Normalized temperature-dependent PL spectrum for the TASE (dark) and bonded (light) structures.

The bonded structures were characterized using SEM imaging (see Fig. 2(b) and (c)). Since the InP is grown lattice-matched to the sacrificial substrate and based upon previous work on more conventional devices, a high, defect-free material quality can be assumed. As the bonded material is dry etched into the desired shapes, the sidewalls of the hexagonal microdisks are not aligned to a specific crystal orientation. Moreover, the dry etching introduces slight roughness to the sidewalls as can be seen in Fig. 2(c). The horizontal lines visible on the sidewalls correspond to individual cycles during the ICP etching. This physical damage might introduce surface states which can impact the optical characteristics [24] as discussed hereafter.

IV. Optical Characterization

Multiple TASE-grown and bonded microdisks are measured using optical micro-photoluminescence (μPL) spectroscopy. All optical measurements are performed under picosecond-pulsed (78 MHz repetition rate) illumination by a supercontinuum laser at 750 nm (spot size $\sim$1 μm). A 100$\times$ objective is used to focus the light from the top onto the sample as well as to collect the emission from the sample. Here, we discuss the optical results obtained from the devices depicted in Fig. 2. PL spectra shown in Fig. 4 reveal a spontaneous emission centered around 880 nm for the TASE structures and around 900 nm for the bonded ones. At room temperature (RT), the spectral full-width at half maximum (FWHM) is slightly larger for the bonded material ($\sim$60 nm) than for the TASE grown material ($\sim$50 nm). A possible explanation for the slightly increased FWHM of the bonded structures could be the presence of surface states introduced by dry etching since the sidewalls are defined lithographically and therefore, not etched along the crystal facets [24]. The TASE structures on the other hand, intrinsically end up with atomically smooth <110> facets. Epitaxially-grown structures similar to our TASE hexagons suggest only weak influence of the surface on the carrier lifetime even without additional surface passivation [25]. Fig. 5(a) depicts the PL spectra of both samples at increasing excitation fluences. The resonant mode of

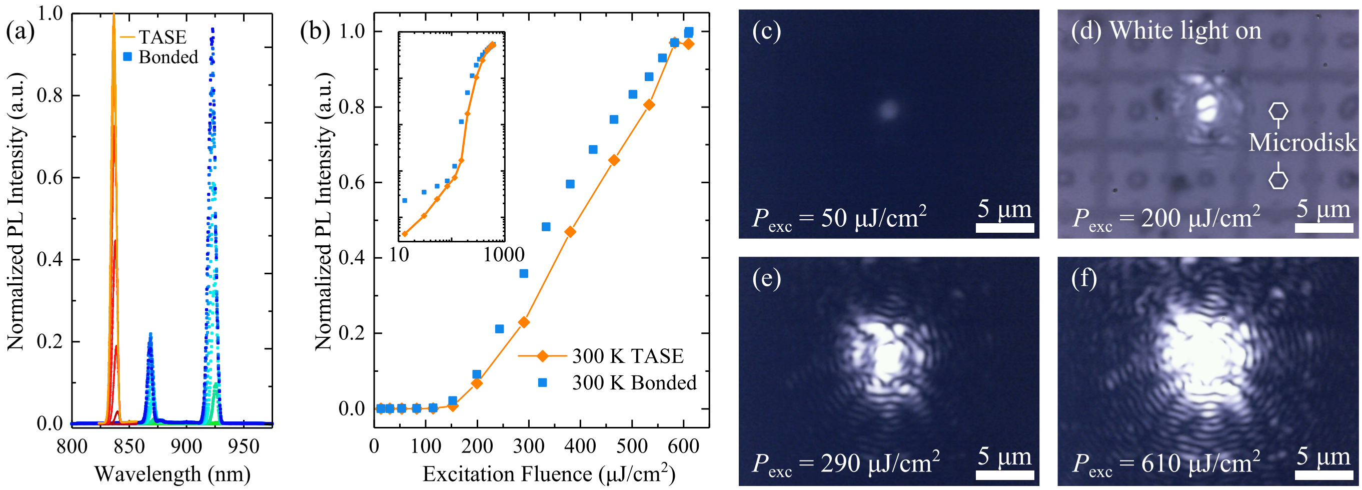

Fig. 5. (a) RT PL spectrum of TASE (line) and bonded (dotted) microdisk lasers under increasing excitation powers. (b) Linear plot of the LL curve of both the TASE (orange diamonds) and bonded (blue squares) samples at RT. The inset shows the LL-curves in a log-log scale. (c)-(f) Optical far field of the TASE structure at different excitation powers: (c) below threshold; (d) at threshold; (e) & (f) above threshold. (d) is taken with white light illumination of the sample.

the TASE microdisk is at 840 nm and the bonded structure exhibits two modes at 880 nm and 926 nm. With increasing pump fluence, both samples show strong, narrow peaks rising from the spontaneous emission background (see Fig. 7(a) at 300 K), which we attribute to lasing.

We performed three-dimensional finite-difference time-domain (3D-FDTD) simulations using *Lumerical* software. The simulated structures include the entire layer stack as depicted in Fig. 1(b), i.e., the Si, InP and surrounding oxide, and the symmetric hexagonal shape shown in Fig. 2. We observed several cavity modes overlapping the gain spectral range featuring theoretical quality factors up to 200.

Fig. 5(b) depicts typical light-in light-out (LL) curves corresponding to the cavity modes centered at 840 nm (TASE sample) and 920 nm (bonded sample). A clear kink marks the onset of the lasing in both samples. The lasing threshold is determined by extrapolating the linear fit above threshold of the linear LL-curve. For the TASE structure we find a threshold fluence of $\sim$200 μJ/cm^2, for the bonded structure a value of $\sim$170 μJ/cm^2. Hence, both samples exhibit similar threshold fluences. Moreover, the slopes of the individual LL-curves are comparable, indicating a similar lasing efficiency of the two samples. The logarithmic plot of the LL-curves is shown in the inset of Fig. 5(b) featuring a clear S-shape. Additionally, the images in Fig. 5(c)–(f) show the far-field images of the light emission (TASE sample) captured with a standard camera and an 800 nm long-pass filter. At low fluence, spontaneous emission is visible (Fig. 5(c)). With increasing pump power, the emission becomes much stronger and fringes start to form (Fig. 5(d) and (e)). Under strongest excitation, many interference fringes in the far-field radiation pattern are observed as a consequence of the extended first-order coherence of the laser emission (see Fig. 5 (f)).

We investigated the lasing behavior of several TASE-grown and bonded microdisk cavities. All the structures measured across both samples exhibit very similar lasing characteristics. The wavelength of the lasing mode can be varied by changing

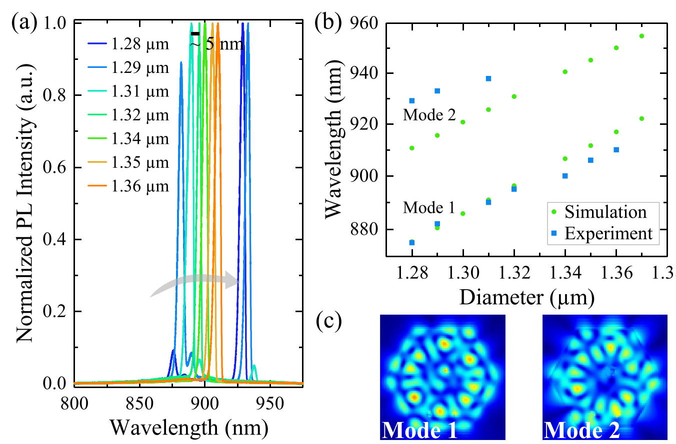

Fig. 6. (a) PL emission of bonded hexagonal structures with varying cavity diameter. The lasing mode shifts to longer wavelengths with increasing hexagon diameter. (b) Center wavelength of the lasing mode versus the diameter of measured (blue squares) and simulated (green dots) hexagonal microdisks. Simulations are performed on symmetric hexagons.

the diameter of the structures. During the TASE process, this can be achieved by adjusting the growth duration or modifying the template design. However, the bonded structures allow for a more straightforward, faster comparison and offer a higher variety of shapes. We varied the size of the bonded hexagonal microdisk from 1.28 μm to 1.36 μm to demonstrate the capability of wavelength tunability (see Fig. 6(a)). PL spectroscopy is performed on all fabricated sizes, revealing a continuous, linearly increasing red-shift of the lasing mode with increasing diameter of the cavity. 3D-FDTD simulations confirm the magnitude of the measured wavelength shift with increasing microdisk diameter (see Fig. 6(b)). Fig. 6(c) shows the simulated mode profile of Mode 1 and 2 depicted in Fig. 6(b).

To further assess the material quality on both samples, we perform temperature-dependent measurements between 10 K and

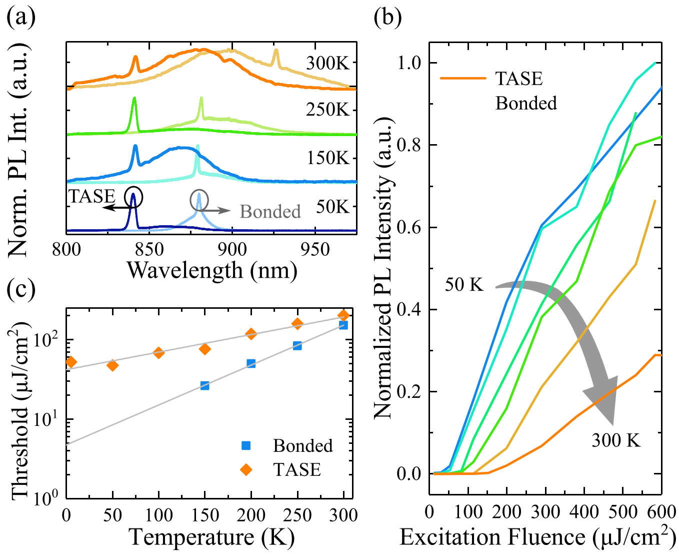

Fig. 7. (a) PL-emission spectrum above threshold at different temperatures for both, TASE (dark) and bonded (bright) structure. (b) Temperature-dependent LL-curves for the TASE-grown InP microdisk. (c) Lasing threshold versus temperature (ln plot) for the two samples. The linear fits are used to determine the characteristic temperatures T_0.

300 K. At low temperatures, the emission shifts to lower wavelengths following the Varshni shift (see Fig. 4). Compared to the RT measurements, the FWHM of the spontaneous emission peak of the TASE structure is slightly wider than the bonded PL FWHM. We believe that the narrowing of the FWHM of the bonded sample with decreasing temperature can be attributed to surface states. The TASE sample on the other hand, exhibits twin planes and both, zincblende and wurtzite segments (see Fig. 3(e) and (f)). This potentially leads to an inhomogeneously broadened PL emission independent of temperature [12], [26]. The lasing mode of the TASE structure stays at 840 nm as the gain shifts with temperature. The bonded structure shows two modes at RT as depicted in Fig. 5(a). When going to lower temperatures, the material gain shifts to lower wavelengths and hence, the spectral overlap with the mode at 926 nm decreases while the overlap at 880 nm increases. Therefore, the dominant lasing mode changes from 926 nm to 880 nm around 250 K (see Fig. 7(a)). The linear LL-curves for the TASE samples at temperatures between 50 K and 300 K measured in 50 K steps are depicted in Fig. 7(b). By plotting the lasing threshold versus temperature in Fig. 7(c), the characteristic temperature T_0 of the devices can be extracted by fitting data to the empirical relation $P_{\mathrm{th}}(T) \propto \exp(T/T_0)$. The TASE microdisk exhibits a T_0 of $\sim$190 K and the bonded structure of $\sim$90 K. Interestingly, the bonded material reveals a much lower characteristic temperature than the TASE structure. As mentioned, we believe that surface states could be responsible for this behavior. The characteristic temperature of the TASE microdisk on the other hand, is comparable to values achieved in III-V quantum dot disk lasers [7], [27]. Moreover, it is comparable to our previously reported low temperature InGaAs microdisk lasers that has also been fabricated using a TASE-based approach [20].

TABLE I
COMPARISON OF INTEGRATION METHODS IN THIS WORK

	Direct Wafer Bonding	**Template-Assisted Selective Epitaxy**
Wafer Size	Limited	300 mm
Growth Direction	Vertical direction	Lateral direction
Preferred Embedding of QWs	Parallel to substrate	Orthogonal to substrate
In-plane Integration with Si	No	Yes
Co-integration with Different III-Vs	Limited	Demonstrated [29]
Defects	Surface	Twin planes
Shape Control	Etching	By growth
Lasing Performance		
T_0 [K]	~90	~190
$P_{\mathrm{th,\,300\,K}}$ [µJ/cm²]	~170	~200
LL-curve $_{300\,\mathrm{K}}$	Comparable	

V. DISCUSSION AND CONCLUSION

We demonstrated RT lasing from InP microdisks monolithically integrated on Si by TASE epitaxial growth and compared their performance to identical devices fabricated by conventional wafer bonding and etching. Traditionally, InP is an important material for III-V photonics because it enables the integration of lattice-matched QWs at telecom wavelengths, however due to the large lattice mismatch it is also a challenging material to grow directly on silicon. The obtained lasing performance of the TASE devices compares well with the bonded InP microdisks. The RT PL signal is narrower for the TASE devices, however, they show a slightly higher threshold power but a greater T_0 value. Morphological investigation by STEM analysis, shows that the material grown by TASE is single crystalline and of high quality without any threading dislocations in the active gain region. Additionally, our TASE structures inherently grow with atomically smooth crystal side facets which should result in a reduction of the number of dangling bonds and defects at the surface. The attributes of the two approaches are listed in Table I. Compared to the mature bonding technology, our presented TASE approach offers the extra advantage of growing in lateral direction and hence, allows for new device concepts and integration schemes. Whereas typical QWs are grown parallel to the substrate, TASE growth proceeds radially from the center outwards and thereby offers an interesting opportunity to incorporate QWs and doping profiles. For example, using TASE, in-situ doped regions can be integrated in-plane, favoring p-i-n structures parallel to the Si substrate which allow for compact electrical pumping schemes [28]. Moreover, QWs can be integrated orthogonal to the substrate, therefore favoring new device concepts. The placement and geometry of the TASE structures are defined by a combination of lithography, template design, and growth duration. Hence, it enables a dense integration with silicon electronics and passive optics. When working on an SOI platform as in [20], the TASE approach supports in-plane integration with Si. Using the same technique, by repeated growth runs, we have also demonstrated the dense local integration of different III-V families on the same silicon wafer [29].

In conclusion, we presented a promising approach for monolithic integration of III-V microdisk lasers on Si. By demonstrating InP microdisk lasers with high material quality, we pave the way for future embedding of lattice-matched QWs and hence, the fabrication of efficient microdisk lasers emitting above the silicon band edge.

Acknowledgment

The authors gratefully acknowledge P. Staudinger, P. Tiwari, M. D. Rossell, and J. Leuthold for fruitful technical discussions, as well as, the BRNC staff for technical support.

References

[1] D. A. B. Miller, "Optical interconnects to electronic chips," *Appl. Opt.*, vol. 49, no. 25, pp. F59–F70, 2010.

[2] C. Sun *et al.*, "Single-chip microprocessor that communicates directly using light," *Nature*, vol. 528, pp. 534–538, 2015.

[3] O. Marshall *et al.*, "Heterogeneous integration on silicon photonics," *Proc. IEEE*, vol. 106, no. 12, pp. 2258–2269, Dec. 2018.

[4] Z. Zhou, B. Yin, and J. Michel, "On-chip light sources for silicon photonics," *Light, Sci. Appl.*, vol. 4, 2015, Art. no. e358.

[5] G. Morthier, T. Spuesens, P. Mechet, G. Roelkens, and D. Van Thourhout, "InP microdisk lasers integrated on Si for optical interconnects," *IEEE J. Sel. Topic Quantum Electron.*, vol. 21, no. 6, 2015, Art. no. 1500610.

[6] G. Crosnier *et al.*, "Hybrid indium phosphide-on-silicon nanolaser diode," *Nature Photon.*, vol. 11, pp. 297–300, 2017.

[7] B. Shi *et al.*, "1.55 μm room-temperature lasing from subwavelength quantum-dot microdisks directly grown on (001) Si," *Appl. Phys. Lett.*, vol. 110, no. 12, 2017, Art. no. 121109.

[8] Y. Wan *et al.*, "O-band electrically injected quantum dot micro-ring lasers on on-axis (001) GaP/Si and V-groove Si," *Opt. Express*, vol. 25, no. 22, pp. 26853–26860, 2017.

[9] Y. Wan *et al.*, "13 μm submilliamp threshold quantum dot micro-lasers on Si," *Optica*, vol. 4, no. 8, pp. 940–944, 2017.

[10] B. Mayer *et al.*, "Monolithically integrated high-β nanowire lasers on silicon," *Nano Lett.*, vol. 16, no. 1, pp. 152–156, 2016.

[11] F. Schuster, J. Kapraun, G. N. Malheiros-Silveira, S. Deshpande, and C. J. Chang-Hasnain, "Site-controlled growth of monolithic InGaAs/InP quantum well nanopillar lasers on silicon," *Nano Lett.*, vol. 17, no. 4, pp. 2697–2702, 2017.

[12] Z. Wang *et al.*, "Room-temperature InP distributed feedback laser array directly grown on silicon," *Nature Photon.*, vol. 9, pp. 837–842, 2015.

[13] B. Kunert *et al.*, "III/V nano ridge structures for optical applications on patterned 300 mm silicon substrate," *Appl. Phys. Lett.*, vol. 109, no. 9, 2016, Art. no. 091101.

[14] C. Merckling *et al.*, "Heteroepitaxy of InP on Si(001) by selective-area metal organic vapor-phase epitaxy in sub-50 nm width trenches: The role of the nucleation layer and the recess engineering," *J. Appl. Phys.*, vol. 115, no. 2, 2014, Art. no. 023710.

[15] Z. Wang *et al.*, "Polytypic InP nanolaser monolithically integrated on (001) silicon," *Nano Lett.*, vol. 13, no. 11, 5063–5069, 2013.

[16] M. Borg *et al.*, "Vertical III-V nanowire device integration on Si(100)," *Nano Lett.*, vol. 14, no. 4, pp. 1914–1920, 2014.

[17] L. Czornomaz *et al.*, "Confined Epitaxial Lateral Overgrowth (CELO): A novel concept for scalable integration of CMOS-compatible InGaAs-on-insulator MOSFETs on large-area Si substrates," in *Proc. Symp. VLSI Technol*, 2015, pp. T172–T173.

[18] S. Mauthe *et al.*, "Monolithic integration of III-Vs on silicon for electronic and photonic applications," presented at the MNE, 08-11-01, 2018.

[19] S. Wirths *et al.*, "Room-temperature lasing from monolithically integrated GaAs microdisks on silicon," *ACS Nano*, vol. 12, no. 3, 2169–2175, 2018.

[20] S. Mauthe *et al.*, "Monolithically integrated InGaAs microdisk lasers on silicon using template-assisted selective epitaxy," *Proc. SPIE*, vol. 10672, 2018, Art. no. 106722U.

[21] Y. Baumgartner *et al.*, "Monolithic integration of InAlAs/InGaAs quantum-well on InP-OI micro-substrates on Si for infrared light sources," *Proc. IEEE 14th Int. Conf. Group IV Photon.*, 2017, pp. 173–174.

[22] J. E. Ayers, *Heteroepitaxy of Semiconductors: Theory, Growth, and Characterization*, Boca Raton, FL, USA: CRC Press, 2007, pp. 17–19.

[23] D. Caimi, C. B. Zota, C. Convertino, and L. Czornomaz, "Direct wafer bonding of III-V layers on processed wafers for 3D sequential integration," presented at the MNE, 08-11-03, 2018.

[24] A. Higuera-Rodriguez *et al.*, "Ultralow surface recombination velocity in passivated InGaAs/InP nanopillars," *Nano Lett.*, vol. 17, no. 4, pp. 2627–2633, 2017.

[25] H. J. Joyce *et al.*, "Ultralow surface recombination velocity in InP nanowires probed by terahertz spectroscopy," *Nano Lett.*, vol. 12, no. 10, pp. 5325–5330, 2012.

[26] P. Staudinger, S. Mauthe, K. E. Moselund, and H. Schmid, "Concurrent zinc-blende and wurtzite film formation by selection of confined growth planes," *Nano Lett.*, vol. 18, no. 12, 7856–7862, 2018.

[27] Y. Wan *et al.*, "Temperature characteristics of epitaxially grown InAs quantum dot micro-disk lasers on silicon for on-chip light sources," *Appl. Phys. Lett.*, vol. 109, no. 1, 2016, Art. no. 011104.

[28] S. Sant *et al.*, "Modeling whispering gallery mode III-V micro-lasers monolithically integrated on Silicon," in *Proc. Int. Conf. Numer. Simul. Optoelectron. Devices*, 2018, pp. 79–80.

[29] M. Borg *et al.*, "High-mobility GaSb nanostructures cointegrated with inas on Si," *ACS Nano*, vol. 11, no. 3, pp. 2554–2560, 2017.

Svenja Mauthe received the B.S. and M.S. degrees in physics from the Karlsruhe Institute of Technology, Karlsruhe, Germany, in 2012 and 2016, respectively. She is currently working toward the Ph.D. degree in electrical engineering with the Eidgenössische Technische Hochschule, Zurich, Switzerland in collaboration with IBM Research Zurich, Switzerland. Her research focuses on the epitaxial integration of III-V microlasers on silicon.

Noelia Vico Triviño received the M.S. and Ph.D. degrees from the University of Granada, Granada, Spain, and the École Polytechnique Fédérale de Lausanne, Lausanne, Switzerland, respectively. In 2018, she joined IBM Research-Zurich, where she is currently working on the integration of III–V semiconductors on silicon for photonic applications. In 2015, she was awarded a Career Grant by the Swiss National Science Foundation to continue her research with the Massachusetts Institute of Technology, USA.

Yannick Baumgartner received the B.Sc. and M.Sc. degrees in materials science from the Ecole polytechnique fédérale de Lausanne, Lausanne, Switzerland, in 2013 and 2016, respectively. Shortly after, he joined the IBM Research–Zurich Laboratory, Switzerland, where he is currently working toward the Ph.D. degree on the integration of III–V lasers on silicon using wafer bonding and selective epitaxy.

Marilyne Sousa received the M.S. degree in optics and photonics from the University of Orsay, Orsay, France, in 1998. She joined the IBM Zurich Research Laboratory in 2000 where she was involved in various projects ranging from the optimization of OLED materials to the optimization of oxides or III–Vs for various applications. She is currently responsible for thin films material characterization using spectroscopic ellipsometry and transmission electron microscopy.

Daniele Caimi is a Senior Technical Specialist with the IBM Zurich Research Laboratory, which he joined in 2001. Till 2003, he has worked for the Photonic group in the fabrication of SiON optical waveguides. In 2004, he joined the Advanced Functional Materials Group, working on silicon and III/V gate stack materials done by molecular beam epitaxy. In 2014, he moved to the Materials Integration Nanoscale Devices group, working on III–V material integration on Si platform. His current technical responsibilities are development and process of III–V and Silicon CMOS compatible devices. Prior to joining IBM, he was responsible for the technological aspects and fabrication of telecomunication relais bei Axicom in Au (ZH), Switzerland.

Thilo Stöferle received the M.S. degree in physics from the University of Heidelberg, Heidelberg, Germany, in 2001, the Ph.D. degree in quantum optics from the Eidgenössische Technische Hochschule (ETH), Zürich, Switzerland, in 2005. Since 2006, he has been working with IBM Research—Zurich first as Postdoc and since 2007 as a Permanent Research Staff Member. His current research interests are quantum computing and simulation and light-matter interaction in nanophotonic cavities with quantum materials. He was the recipient of the ETH Medal in 2005 and the Dimitris N. Chorafas Award in 2006. Since 2000, he has been a member of the German Physical Society and since 2017 he has been a member of the executive board of the Swiss Physical Society.

Heinz Schmid received the Diploma in physics in 1988. He is a Senior Engineer. He authored more than 100 papers in refereed journals. His current research areas comprise integration of III–V compounds on Si, design and fabrication of scaled III-V devices with a focus on transistors, quantum devices, and lasers. He was the recipient of the Erwin W. Mueller Outstanding Young Scientist Award in 1992.

Kirsten Emilie Moselund received the M.Sc. degree in engineering from the Technical University of Denmark, Lyngby, Denmark, in 2003 and the Ph.D. degree in microelectronics from the Swiss Federal Institute of Technology in Lausanne, Lausanne, Switzerland, in 2008. In 2008, she joined the IBM Zurich——Research, where she is currently managing the Materials Integration and Nanoscale Devices group, which among other things focuses on the development of III–V on silicon monolithic integration for novel electronic and photonic device concepts. Her research interests include nanofabrication technology, semiconductor physics, nanophotonics and novel electronic, and photonic device concepts.